Structural Dynamics of Myoglobin: Spectroscopic and Structural Characterization of Ligand Docking Sites in Myoglobin Mutant L29W†

Karin Nienhaus,‡ Pengchi Deng,‡ Jan M. Kriegl,‡ and G. Ulrich Nienhaus*,‡,§

Department of Biophysics, University of Ulm, 89069 Ulm, Germany, and Department of Physics, University of Illinois at Urbana-Champaign, Urbana, Illinois 61801

Received May 14, 2003; Revised Manuscript Received June 21, 2003

ABSTRACT: We have studied CO binding to the heme and CO migration among protein internal cavities after photodissociation in sperm whale carbonmonoxy myoglobin (MbCO) mutant L29W using Fourier transform infrared (FTIR) spectroscopy combined with temperature derivative spectroscopy (TDS) and kinetic experiments at cryogenic temperatures. Photoproduct intermediates, characterized by CO at particular locations in the protein, were selectively enhanced by applying special laser illumination protocols. These studies were performed on the L29W mutant protein and a series of double mutants constructed so that bulky amino acid side chains block passageways between cavities or fill these sites. Binding of xenon was also employed as an alternative means of occluding cavities. All mutants exhibit two conformations, A_I and A_{II}, with distinctly different photoproduct states and ligand binding properties. These differences arise mainly from different positions of the W29 and H64 side chains in the distal heme pocket [Ostermann, A., *et al*. (2000) *Nature 404*, 205−208]. The detailed knowledge of the interplay between protein structure, protein dynamics, and ligand migration at cryogenic temperatures allowed us to develop a dynamic model that explains the slow CO and O_2 bimolecular association observed after flash photolysis at ambient temperature.

Myoglobin (Mb),[1] a small, structurally well characterized globular protein with a comparatively simple function, has served as a paradigm for structure−dynamics−function relations in proteins for many years (*1*−*8*). Its 153 amino acids are arranged in eight α-helices surrounding a heme prosthetic group. An Fe^{2+} ion in the center of the heme group binds small ligands such as O_2, CO, and NO. Early on it was realized that the X-ray structure of myoglobin lacked pathways by which ligands could access the active site (*9*−*11*). Consequently, large-scale fluctuations of the structure that open transient channels must be essential for its function.

The iron−ligand bond in MbO_2 and MbCO can be broken by a short laser flash, and the ensuing ligand binding reaction can be followed spectroscopically (*12*). By performing these flash photolysis experiments over wide time and temperature ranges, Frauenfelder and co-workers discovered in the 1970s a surprising complexity in ligand binding to myoglobin (*2*). At cryogenic temperatures, ligands were observed to rebind geminately from within the heme pocket. The nonexponential kinetics of this process were explained by structural heterogeneity and led to the important concept of conformational substates. Furthermore, evidence of a small number of discrete kinetic intermediate states was found. Initially, these were proposed to arise from a series of enthalpy barriers that the ligand must overcome on its way to the active site (*2*). Because of a lack of direct structural evidence, this interpretation was merely speculative and discussed controversially by different groups. Two physically distinct explanations were put forward to explain the complex kinetics. In one class of models, protein conformational changes were suggested to occur upon breakage of the iron−ligand bond (*13*−*18*). Alternatively, different docking sites were assumed, among which ligands can migrate after dissociation from the heme iron (*15*, *19*−*21*). Only in recent years has a consistent structural interpretation of the ligand binding kinetics in myoglobin begun to emerge on the basis of a concerted experimental approach, combining X-ray crystallography of photoproduct intermediates with time-resolved spectroscopy and protein engineering. As will be shown in this work, protein conformational dynamics and ligand migration can both play an important role in ligand binding.

The first MbCO photoproduct X-ray structures were determined after photolysis at <40 K. They revealed the CO in primary docking site B in the vicinity of the heme iron (*22*−*25*). Subsequently, CO was also found in two secondary photoproduct sites, denoted C and D (*26*−*28*), which are identical to two of the four protein internal cavities known to bind xenon (*29*). They are termed the Xe4 (C) and Xe1 (D) cavities. Suggestions have been made about the relevance of these cavities for a possible physiological role of myoglobin as a nitric oxide scavenger (*4*, *30*).

In recent years, X-ray crystallography has also been applied in kinetic studies of photoproduct intermediates (*25*, *31*). These experiments are quite challenging and limited in their sensitivity. In contrast, infrared spectroscopy is a

† This work was supported by the Deutsche Forschungsgemeinschaft (Ni-291/3).

* To whom correspondence should be addressed. E-mail: uli@uiuc.edu.

‡ University of Ulm.

§ University of Illinois at Urbana-Champaign.

[1] Abbreviations: Mb, myoglobin; wt, wild type; FTIR, Fourier transform infrared; TDS, temperature derivative spectroscopy.

10.1021/bi034787s CCC: $25.00
Published on Web 07/23/2003

powerful tool for studying dynamic processes with high sensitivity and time resolution, provided that a suitable marker band exists. The stretch absorption of CO at ~5 μm in heme proteins is a superb marker band because it absorbs strongly and, moreover, it is highly sensitive to the local CO environment (*32*). In CO-ligated sperm whale Mb, three discrete stretch bands can be distinguished for the bound ligand; they are associated with conformational substates A_0, A_1, and A_3 (*33*, *34*). They have different local structural environments at the active site, with different electric fields affecting the bond order of the heme-bound CO and thus its stretching frequency (*35*−*39*). For the study of ligand migration, we measure the stretch spectrum of photodissociated CO. It typically displays multiple sharp IR lines, which is indicative of structurally well-defined ligand docking sites inside the protein matrix (*32*, *40*, *41*). The CO stretch absorption provides information beyond that which can be obtained with X-ray crystallography or time-resolved spectroscopy in the heme electronic transitions (*42*). For instance, the X-ray structure of the primary photoproduct B shows only one CO location (*22*, *23*, *25*), whereas the spectrum of the CO stretch typically yields two distinct infrared bands. They arise from Stark splitting of opposite orientations of the CO dipoles with respect to the internal electric field at the primary docking site (*43*, *44*). After migration to secondary sites, the internal probe molecule CO sees a changed local electric field and will thus display an altered CO spectrum, as has already been observed for MbCO mutants YQR (*45*), V68F, and L29W (*46*, *47*). The appearance of multiple bands shows that the ligand can assume a small number of preferential orientations (frequently two) within each photoproduct site. The CO dynamics within an internal protein cavity can be analyzed from the temperature dependence of the IR spectra (*48*).

In this paper, we will focus on IR studies of ligand migration in myoglobin mutant L29W, for which the X-ray structures of secondary photoproduct states have been determined (*26*). This mutant is particularly interesting because of its very small ligand association rate at room temperature (*36*). At pH >7, the L29W MbCO displays two bands of the CO stretch, denoted A_I (1945 cm^{-1}) and A_{II} (1955 cm^{-1}) (*26*, *49*). This nomenclature was introduced to clearly distinguish these substates from conformational substates A_0, A_1, and A_3 of the native protein. A_0 has been associated with a protonated H64 swinging out of the distal pocket (*50*, *51*). A corresponding band appears in L29W MbCO only at pH <6. To avoid this additional complication, we have limited this study to high-pH samples (pH >7). The relative populations of A_I and A_{II} depend sensitively on temperature and solvent environment. In crystals and glycerol/buffer mixtures, A_I dominates at cryogenic temperatures (<200 K). From 200 to 300 K, the level of A_{II} gradually increases, and it is the main substate at 300 K (*47*). In contrast, A_I remains the majority substate in aqueous buffer even at 300 K.

Figure 1 shows the essential features of the active site structure of L29W MbCO, as determined at 105 K (*26*). For the A_I conformation, the W29 and H64 side chains are depicted in light gray. Alternative positions of these side chains, shown in dark gray, are associated with the photoproduct created by photolysis at >180 K, in which all CO ligands have escaped from the distal heme pocket. The majority of them are recovered at the Xe1 site (D). Apparently, after the escape of the ligand from the distal heme pocket, the A_I structure relaxes to the equilibrium deligated (deoxy) structure, in which the W29 indole side chain assumes a conformation similar to that in the room-temperature ligand-bound state (*52*). It is hence reasonable to associate the A_{II} substate with the W29 indole side chain in this position. Four CO molecules are depicted in Figure 1 (labeled A−D), representing CO ligands in the A_I-bound conformation (A), in the primary photoproduct site (B), in the Xe4 cavity (C), and in the Xe1 cavity (D).

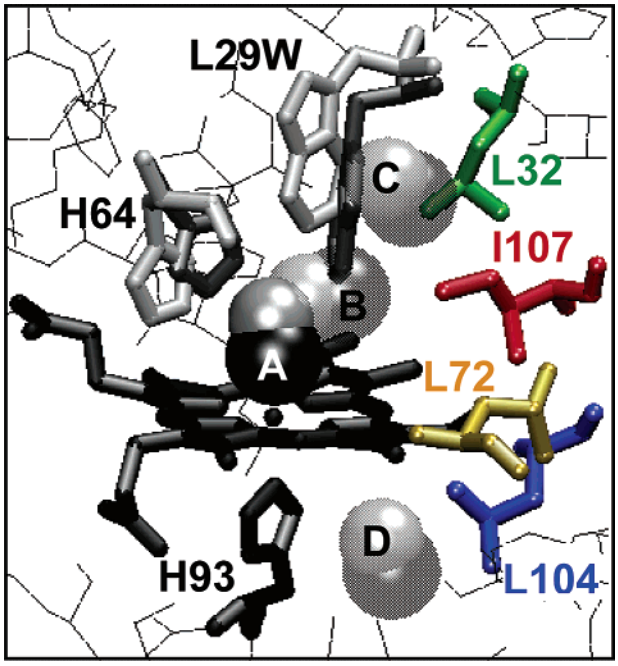

FIGURE 1: Essential features at the active site of myoglobin mutant L29W MbCO. Residues W29 and H64 of taxonomic substates A_I and A_{II} are depicted in light gray and dark gray, respectively. The (wt) side chains of residues 32, 72, 104, and 107 are included in color. CO ligands are shown in the A_I-bound conformation (A), in the primary photoproduct site (B), in the Xe4 cavity (C), and in the Xe1 cavity (D).

To elucidate the dynamic aspects of the ligand binding reaction, particularly CO migration between the xenon cavities, we have performed Fourier transform infrared (FTIR) spectroscopy, temperature derivative spectroscopy (TDS), and isothermal kinetic experiments on L29W MbCO samples modified to markedly influence accessibilities of docking sites and migration pathways. To this end, two strategies have been pursued. (i) MbCO samples were equilibrated with 1 atm of Xe gas. If intermediate CO docking sites are identical with Xe binding sites, Xe atoms and photolyzed CO are expected to compete for them, and the occupancy with CO should decrease. (ii) L29W (double) mutants in which bulky amino acid side chains block docking sites and change migration pathways were constructed. This strategy involves the implicit assumption (which we found to be valid in most of the cases) that single mutations cause local changes and do not disturb the overall architecture of the protein. The choice of mutants was based on molecular modeling and also guided by results of molecular dynamics simulations (*53*), which showed that ligands collided many times with particular residues lining the migration pathways after photolysis. From the large number of mutants that were

studied, we present data on L29W/L72F (modified Xe2 cavity), L29W/L104W (blocked Xe1 cavity), and L29W/L32T and L29W/I107W (modified Xe4 cavity). The (wt) side chains of residues 32, 72, 104, and 107 are shown in Figure 1.

Sophisticated illumination protocols were employed to selectively populate photoproduct states to characterize them individually and to observe ligand migration at cryogenic temperatures. To connect these results to physiological ligand binding, we will present room-temperature flash photolysis data for several of the mutants using both O_2- and CO-ligated samples.

MATERIALS AND METHODS

Site-Directed Mutagenesis, Protein Expression, and Purification. The plasmid carrying the sperm whale myoglobin gene of the L29W mutant was a kind gift of J. S. Olson (Rice University, Houston, TX). All double mutants of L29W used in this work were constructed on the basis of this vector using the Quikchange mutagenesis kit (Stratagene Europe, Amsterdam, The Netherlands) following the manufacturer's protocol. Custom-designed primers were ordered from MWG (MWG-Biotech GmbH, Ebersberg, Germany). Mutant sperm whale myoglobins were expressed in *Escherichia coli* (strain Tb1) and purified as described previously (*54*).

Sample Preparation. For the FTIR experiment, lyophilized myoglobin was dissolved in a 75%/25% (v/v) glycerol/buffer mixture [1 M potassium phosphate (pH 8)] to a final concentration of ~20 mM. Solutions were equilibrated with 1 atm of CO and reduced by adding a 2-fold excess of sodium dithionite (final pH of 7.5). To prepare Xe-bound MbCO samples, the MbCO solutions were stirred for an additional 1 h at 0 °C under 1 atm of Xe gas. To remove any undissolved protein, the sample solution was centrifuged prior to being loaded into the sample cell.

UV−visible spectra and kinetics were recorded for dilute samples, prepared by dissolving the lyophilized protein in 100 mM sodium phosphate buffer (pH 8) to a final concentration of ~10 μM. For MbCO samples, the solutions were equilibrated with 1 atm of CO, and a 10-fold excess of sodium dithionite was subsequently added under anaerobic conditions. MbO_2 samples were prepared by adding dithionite to ferric Mb solutions, which were submitted to a Sephadex G25 column to remove excess reducing agent.

Infrared Spectroscopy. A few microliters of the protein solution was held between two CaF_2 windows (diameter of 25.4 mm) separated by a 75 μm thick Mylar washer. The windows were sandwiched inside a block of oxygen-free high-conductivity copper mounted on the coldfinger of a closed-cycle helium refrigerator (model SRDK-205AW, Sumitomo, Tokyo, Japan). The sample temperature was measured with a silicon temperature sensor diode and regulated in the range of 3−320 K by a digital temperature controller (model 330, Lake Shore Cryotronics, Westerville, OH). A continuous-wave, frequency-doubled Nd:YAG laser (model Forte 530-300, Laser Quantum, Manchester, U.K.), emitting an output power of 300 mW at 532 nm, was used to photolyze the sample. The laser beam was split and focused with lenses on the sample from both sides. The standard photolysis rate k_L was determined to be ~20 s^{-1} at low temperatures. Transmission spectra were collected between 1800 and 2400 cm^{-1} at a resolution of 2 cm^{-1} using a Fourier transform infrared (FTIR) spectrometer equipped with an InSb detector (IFS 66v/S, Bruker, Karlsruhe, Germany).

Isothermal IR Kinetics. FTIR transmission spectra were recorded continuously, while the sample was exposed to laser light for an extended period of time (e.g., 15 000 s) at selected fixed temperatures to produce a nonequilibrium state. Considering a model with only two states, bound state A and photodissociated intermediate state B, we can calculate the photolyzed fraction in the steady state at a particular temperature, $N(T)$, according to (*17*)

$$N(T) = \int \frac{k_L}{k_L + k_{BA}} g(H_{BA})\, dH_{BA} \qquad (1)$$

Here, k_L and k_{BA} are the photolysis and recombination rate coefficients, respectively. If tunneling is neglected, the temperature dependence of the rebinding rate coefficient is given by the Arrhenius law, $k_{BA} = A_{BA}(T/T_0)\exp(-H_{BA}/RT)$, with preexponential factor A_{BA}, activation enthalpy H_{BA}, gas constant R, and reference temperature T_0 (100 K). Integration over enthalpy barriers, weighted by the normalized barrier distribution $g(H_{BA})$, takes the heterogeneous nature of the barrier at the heme iron into account. Within the two-state analysis, the photolyzed fraction should reach a steady state after an illumination time t which is equal to $1/(k_L + k_{BA})$. Instead, extended illumination of heme proteins often yields a slow, logarithmic increase in the photolyzed fraction, which calls for a more complicated kinetic scheme (*16*, *17*). Protein−ligand systems initially trapped in docking site B are excited by a second photon, the energy of which enables them to explore states with higher recombination barriers and, therefore, slower rebinding. Here we have monitored rebinding from these slow states after extended illumination for up to 50 000 s.

Temperature Derivative Spectroscopy (TDS). TDS is an experimental protocol for studying thermally activated rate processes that involve enthalpy barrier distributions (*17*, *41*, *55*). This two-dimensional technique disperses the experimental data not only along the wavenumber axis but also according to the temperature at which the molecules rebind. Initially, a nonequilibrium intermediate state is created by photolysis. The subsequent TDS measurement records the relaxation of the sample back to equilibrium, while the temperature is ramped up linearly with time in the dark. In the experiments reported here, we have used a heating rate β of 5 mK/s, and an FTIR transmission spectrum $I(\nu,T)$ was acquired every 200 s and thus every kelvin. As the temperature increases, rebinding occurs sequentially with respect to the height of the enthalpy barriers. At the lowest temperatures, only proteins with small enthalpy barriers at the heme iron recombine, and with increasing temperatures, successively higher barriers can be surmounted.

In the simplest analysis of TDS data, one assumes that all spectral changes arise from recombination. The absorbance change is set proportional to the rebinding population [$\Delta A(\nu,T) \propto \Delta N(T)$]. If temperature-dependent spectral changes occur in the absence of rebinding, for instance, intrinsic band shifts, they can be removed from the data by appropriate referencing to background spectra recorded separately (*56*). For a simple unimolecular reaction, the

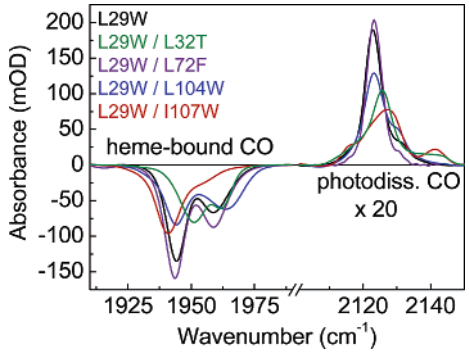

FIGURE 2: FTIR absorbance difference spectra of MbCO L29W and related double mutants (illumination for 1 s at 3 K) in the spectral regions of heme-bound and photodissociated CO.

distribution of barriers, $g(H)$, can be extracted from the first derivative of the population with respect to temperature, $dN(T)/dT$, which is approximated by calculating absorbance difference spectra from transmission spectra at successive temperatures $[\Delta A(\nu,T) = I(\nu,T+{}^1/_2K) - I(\nu,T-{}^1/_2K)]$. In this work, we will present the TDS data conveniently using contour plots, with solid lines indicating an absorbance increase and dashed lines a decrease. For a two-state reaction, the temperature axis can be cast into an enthalpy axis, with the barrier height approximately proportional to the ramp temperature (*17*, *41*, *55*).

Flash Photolysis Experiments. Measurements were carried out in a home-built flash photolysis apparatus on dilute samples sealed in an airtight 1 cm × 1 cm × 3 cm glass cuvette. Photolysis was achieved using a 6 ns (full width at half-maximum) pulse from a frequency-doubled Nd:YAG laser (Surelite 10, Continuum, Santa Clara, CA). Ligand binding was monitored with light from a tungsten source that was passed through a monochromator set at 436 nm. A photomultiplier tube (R5600U, Hamamatsu Corp., Middlesex, NJ) measured the intensities. These data were recorded with a digital storage oscilloscope (TDS 520, Tektronix, Wilsonville, OR) from 10 ns to 50 μs and a home-built logarithmic time-base digitizer (Wondertoy II) from 2 μs to 100 s.

For each kinetic trace, 500 transients were measured at 20 °C and averaged. The data were scaled with the Soret peak absorbance to adjust for slight differences in concentration. An additional scaling factor was introduced to account for the lower extinction coefficients of MbO_2 samples with respect to MbCO samples with the identical concentration. Subsequently, all traces were normalized by a common scale factor so that the amplitude of solvent rebinding in wt MbCO was 0.96 (*57*). Rebinding from the solvent was fitted with exponentials. Second-order rate coefficients were calculated from the pseudo-first-order rate coefficient using the following ligand concentrations: 1 mM CO and 1.34 mM O_2.

RESULTS

Spectroscopic Characterization of Primary Docking Site B. FTIR transmission spectra were measured at 3 K before and after a 1 s photolysis from which photoinduced absorbance difference spectra were calculated. They are plotted in Figure 2 for L29W MbCO and double mutants L29W/L104W, L29W/L72F, L29W/L32T, and L29W/I107W. All samples yielded two bound-state CO bands, A_I at lower and A_{II} at higher wavenumbers. In L29W/I107W, A_{II} is only weakly populated. The spectra in the region of photodissociated CO are also similar, with a large peak and a small peak (at 2122 and 2131 cm^{-1}, respectively, for L29W MbCO). For L29W/I107W and L29W/L32T, there are pronounced changes in the positions and widths of the large peak, and a significant population at 2142 cm^{-1} is also apparent. All CO band positions are compiled in Table 1.

To assess the rebinding properties of these samples, TDS experiments were performed after a 1 s photolysis. Similar behavior was found for all mutants (*56*), and therefore, we show only TDS contour plots of L29W in Figure 3a,b. The map in Figure 3a reveals a markedly different temperature dependence of rebinding for the two substates, A_I and A_{II}, which enables us to decompose the photoproduct TDS data in Figure 3b into spectra associated with one A substate or the other. Pronounced rebinding to A_I at ~35 K occurs from two photoproduct states represented by bands at 2122 and 2131 cm^{-1} (Figure 4). An additional population rebinding to A_I is visible at 120 K. It amounts to only 5% of the total population, and thus, the corresponding photoproduct signals cannot be resolved in the map. Recombination to substate A_{II} is observed over a widely distributed temperature range (3−110 K), implying a very broad barrier distribution. Between 70 and 90 K, rebinding occurs exclusively to A_{II}. Therefore, we have calculated the spectrum of the CO stretch of the A_{II} photoproduct by taking the absorbance difference between 70 and 90 K. This procedure yields a broad spectrum with two bands at 2118 and 2125 cm^{-1} (Figure 4).

Characterization of Secondary Docking Site C′. The small fraction of A_I population rebinding at 120 K (Figure 3a) grows upon extended exposure of the sample to light. This effect was examined by taking FTIR transmission spectra continuously for 15 000 s at 3 K while illuminating the L29W MbCO sample. Absorbance difference spectra were calculated by referencing the transmission data against the "dark" transmission spectrum at time zero. The temporal development of selected spectra is plotted in Figure 5. Also shown is the difference spectrum of the sample, referenced against buffer (dashed line in Figure 5a), which reveals that the sample is only partially photolyzed at 3 K, even after illumination for 15 000 s. The photolyzed fraction of substate A_I does not change at all during this time. This implies that the spectrum of rebinding rate coefficients in the A_I ensemble in the range of the excitation rate k_L of ~20 s^{-1} does not change. The measurement is not sensitive to changes in much faster rebinding proteins, which are likely responsible for the observed incomplete photolysis, and much more slowly rebinding ones, which are photolyzed completely anyway. In contrast, the photodissociated fraction of A_{II} increases slightly with time. Hence, for this substate, the fraction of slow rebinders increases. The photoproduct spectrum in Figure 5b shows a distinct evolution with time. The dominant peak at 2122 cm^{-1} shifts toward higher wavenumbers, and a minor peak at 2132 cm^{-1} grows in magnitude.

To obtain insight into the rebinding properties of the photolyzed population, a TDS experiment was performed after illumination for 15 000 s at 3 K. The TDS contour maps of heme-bound and photolyzed CO in panels c and d of Figure 3 display pronounced differences from the maps after a short illumination (Figure 3a,b). Substate A_I recombines from two approximately equal populations at temperatures

Table 1: IR Stretch Band Positions of Heme-Bound and Photodissociated CO in Myoglobin Mutant L29W and Related Double Mutants[a,b]

mutant MbCO	A_I (cm^{-1})	A_{II} (cm^{-1})	$B_1(A_I)$ (cm^{-1})	$B_2(A_{II})$ (cm^{-1})	$B(A_{II})$ (cm^{-1})	C′ (cm^{-1})	C″ (cm^{-1})	D (cm^{-1})
L29W	1945	1958	2131	2122	2118/2125	2127/2133	2130/2135	2128
L29W/L32T	1951	1961	2131/2142/2123[e]		N/A[c]	2123/2132	2123/2132	2128
L29W/L72F[d]	1944	1959	2131	2122	N/A[c]	2128/2133	2130/2135	2128
L29W/L104W	1946	1963	2131	2122	N/A[c]	2127/2133	2130/2135	-
L29W/I107W	1941	1952	2128/2142/2117[e]		N/A[c]	2128/2138	2130/2133	2128

[a] IR band frequencies were determined at 3 K with an estimated experimental error of ±0.5 cm^{-1}. [b] The pH values were determined at room temperature to be 7.5 with an accuracy of ±0.1 pH unit. [c] Band positions of $B(A_{II})$ were not determined. [d] Mutant L29W/L72F shows an additional A-state band at 1915 cm^{-1}. [e] These bands sit on a broad pedestal, and the band at 2142 cm^{-1} is not assigned.

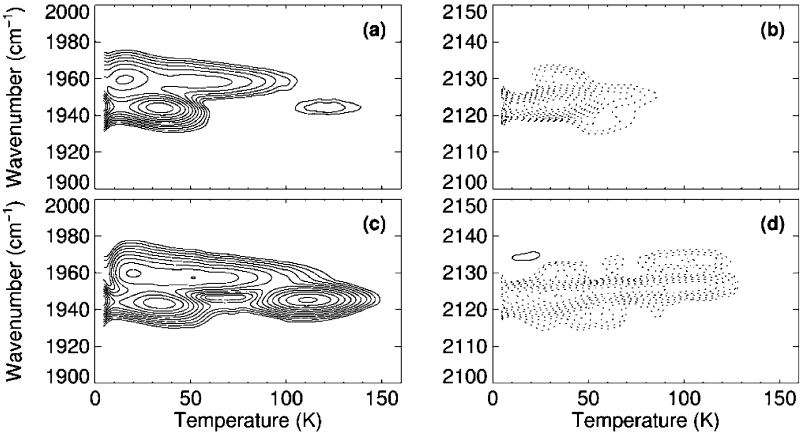

FIGURE 3: TDS contour maps of (a and b) L29W after illumination for 1 s at 3 K and (c and d) after illumination for 15 000 s at 3 K. Absorbance changes in the IR bands of heme-bound CO are plotted in panels a and c; absorbance changes in the photoproduct bands are seen in panels b and d. Contours are spaced logarithmically; solid and dotted lines represent absorbance increases and decreases, respectively.

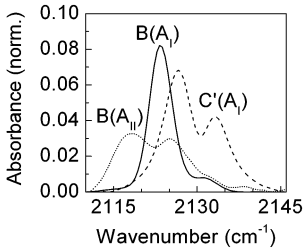

FIGURE 4: Photoproduct spectra of intermediates B and C′. Spectra of the primary photoproduct B were obtained by calculating absorbance differences across the recombination features in Figure 3c: from 30 to 40 K for $B(A_I)$ and from 70 to 90 K for $B(A_{II})$. The spectrum for C′ was calculated as the absorbance difference from 110 to 120 K of the TDS data in Figure 3d.

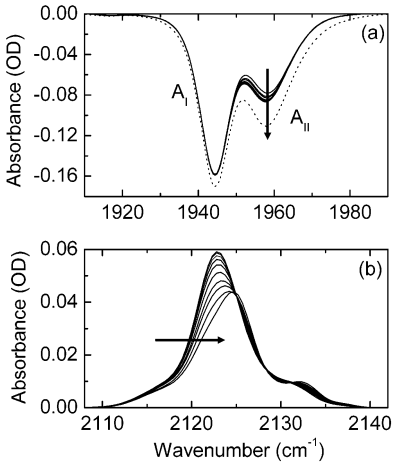

FIGURE 5: Temporal development of FTIR absorbance difference spectra of myoglobin mutant L29W MbCO during illumination for 15 000 s at 3 K: (a) heme-bound CO and (···) total population of the sample and (b) photodissociated CO. Arrows indicate the time progression.

centered around 35 and 110 K. Apparently, ∼50% of the molecules in photoproduct intermediate B have been converted to a new intermediate, denoted C′, in which the CO resides in the Xe4 cavity (*vide infra*) (*26*). For the A_{II} substate, a similar peak at higher temperatures is absent. There is, however, a clearly visible change at the lowest temperatures, where population has been removed, and in the high-temperature tail, which has shifted further up to ∼120 K. This observation supports the conclusion drawn from the data taken while illuminating the sample, namely, that low-barrier (temperature) and hence fast rebinders have shifted to higher barriers (temperature) in A_{II}.

The photoproduct map in Figure 3d is complicated because spectroscopic features from two intermediates recombining to A_I and at least one population rebinding to A_{II} are superimposed. Nevertheless, it is already clear from visual inspection that the IR spectra associated with the A_I photoproduct intermediates rebinding at 35 and 120 K consist of doublets. In Figure 4, we have included the CO spectrum calculated from the TDS data across the rebinding feature of C′ (110−120 K); it exhibits two bands at 2127 and 2133 cm^{-1}. C′ band positions of all samples are listed in Table 1.

The light-induced increase in the level of the C′ intermediate raises questions about the mechanism by which light causes migration of the CO molecule to the Xe4 cavity. In principle, we may suppose that (i) this process occurs by thermal activation (or tunneling) from intermediate B after photodissociation, (ii) electronic excitation of the heme provides energy to the system in intermediate state B to form C′, or (iii) the photodissociation event supplies kinetic energy to the CO that enables it to overcome the barrier to C′. We have addressed these issues by measuring the rebinding

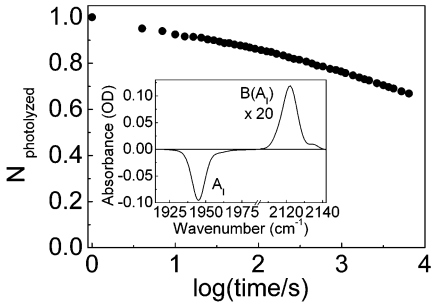

FIGURE 6: Temporal development of the integrated absorbance in the A-state bands of L29W MbCO, monitored at 3 K after illumination for 1 s. The inset shows the overall absorbance change during relaxation for 7000 s.

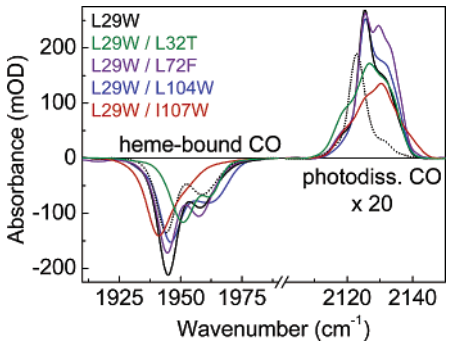

FIGURE 7: FTIR absorbance difference spectra of MbCO L29W samples and related double mutants taken with slow cooling under illumination from 160 to 3 K in the spectral ranges of heme-bound and photodissociated CO. The dotted line is the spectrum of L29W MbCO with illumination for 1 s.

kinetics at 3 K after a 1 s photolysis. Within 7000 s, ~30% of the photolyzed ligands in A_I recombine (Figure 6). During this time, no spectral changes similar to those reported in Figure 5b were observed. Therefore, intermediate C′ is definitely not populated thermally in the absence of light. Moreover, the fact that only a fraction of the ligands rebind in 7000 s (and hence somewhat more in 15 000 s) leads us to conclude that scenario (iii) is also out of the question, because the number of photolysis events does not even increase 2-fold in 15 000 s, which then cannot explain the 50-fold increase in the C′ population. Therefore, electronic excitation of the heme group apparently provides the energy to the CO in docking site B and enables it to migrate to the Xe4 cavity.

Characterization of Intermediate State C″. Figure 7 shows absorbance difference spectra of the identical samples as in Figure 2 after photodissociation using the slow-cool protocol (*17*). They were calculated from transmission spectra after cooling from 160 to 3 K at 5 mK/s under illumination, which were referenced against a spectrum taken after cooling to 3 K in the dark. For comparison, the FTIR spectrum of L29W MbCO at 3 K after illumination for 1 s (dotted line) is also included. The increased absorbance in the A substate bands of L29W MbCO reflects complete photolysis after slow-cool illumination. Comparison of the photoproduct spectra in Figure 7 with those after a 1 s illumination at 3 K (Figure 2) shows that they have completely changed upon slow-cool light exposure. Instead of a strong peak at ~2122 cm^{-1}, the spectrum after slow-cool illumination shows a dominant peak at ~2127 cm^{-1} and a weaker one at ~2133 cm^{-1} for L29W, L29W/L72F (modified Xe2 cavity), and L29W/L104W

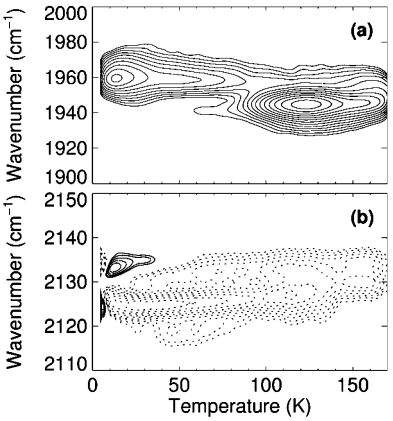

FIGURE 8: TDS contour maps of L29W MbCO after slow cooling from 160 to 3 K: (a) absorbance changes in the IR bands of heme-bound CO and (b) absorbance changes of the photoproduct bands. Contours are spaced logarithmically; solid and dotted lines represent absorbance increases and decreases, respectively.

(blocked Xe1 cavity). Mutants L29W/L32T and L29W/I107W (both have a modified Xe4 cavity) again exhibit markedly different IR spectra.

TDS experiments were performed after slow cooling under light in an effort to examine the rebinding behavior of the photoproduct states created by this photolysis protocol. The A substate map in Figure 8a shows that exclusively A_{II} rebinds below 70 K. Consequently, all CO ligands in Mb molecules of substate A_I have migrated away from initial docking site B to other locations. Rebinding in A_I occurs in the temperature range from 90 to 160 K, with a maximum at 120 K and a pronounced shoulder above 140 K, which suggests that two distinct subpopulations exist. The corresponding photoproduct map (Figure 8b) is somewhat complicated. The solid lines below 30 K represent an exchange of photolyzed population between two IR bands. This effect is frequently observed and related to CO reorientation within a docking site (*46*). Below 80 K, recombination within A_{II} predominantly occurs from a band at 2125 cm^{-1}, and the low-frequency contribution around 2118 cm^{-1} (Figure 4) is also visible. At 120 K, at the peak of C′ rebinding in the A_I conformation, the map reveals two bands at 2127 and 2133 cm^{-1}, which we have already associated with the C′ intermediate (Figure 4). Around 140 K, the contours shift markedly, indicating that the population rebinding in the shoulder of the A substate contours above 140 K constitutes a spectroscopically distinguishable intermediate state, which we denote C″, with the IR bands of the CO stretch at 2130 and 2135 cm^{-1}.

The TDS maps of the double mutants after slow-cool illumination share distinct similarities (*56*). As in L29W MbCO, the A substate maps show recombination to A_{II} with broadly distributed recombination temperatures, from 3 to ~120 K. Recombination to A_I occurs from two subpopulations peaking at ~120 and ~150 K. The spectra of C′ (2127 and 2133 cm^{-1}) and C″ (2130 and 2135 cm^{-1}) of L29W and double mutants L29W/I104W and L29W/L72F (normalized to equal areas) are given in Figure 9a. The similarities are obvious. For L29W/I107W and L29W/L32T (Figure 9b), however, the spectra assigned to C′ and C″ differ considerably from those of L29W, indicating that the replacements at residues 32 and 107 must have altered the local environment of the CO ligand in both intermediate states, C′ *and*

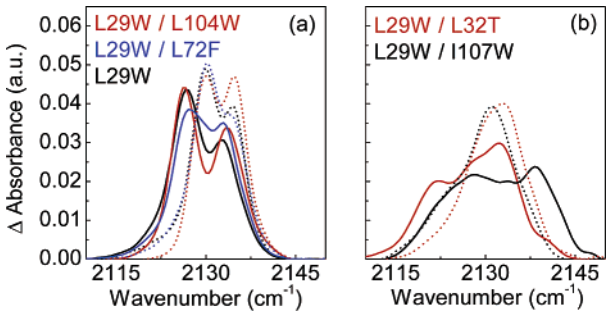

FIGURE 9: Photoproduct spectra associated with intermediates C′ and C″ of L29W and selected double mutants. Absorbance differences were calculated across the recombination features in the TDS maps after slow cooling from 160 to 3 K, taking temperature intervals from 110 to 120 K for C′ and from 150 to 160 K for C″.

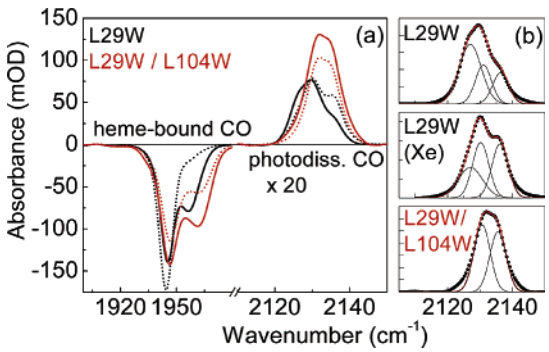

FIGURE 10: (a) FTIR absorbance difference spectra of MbCO samples L29W and L29W/L104W after illumination at 185 K for 2 h and subsequent slow cooling under illumination from 185 to 160 K in the spectral ranges of heme-bound and photodissociated CO. (b) Fits of the photoproduct spectra in panel a with three Gaussian lines at 2128, 2130, and 2135 cm^{-1}.

C″. Table 1 contains the C″ band positions of all the mutants that have been studied.

Photoproduct Intermediates in a Fluctuating Protein. So far, we have characterized photoproducts B, C′, and C″ which are present in a protein essentially arrested by the surrounding solvent glass. To spectroscopically explore the photoproduct intermediate D, in which the CO has migrated to the Xe1 cavity on the proximal side of the heme, MbCO samples were illuminated at 185 K for 2 h. Subsequently, the temperature was ramped to 160 K under light at a rate of 5 mK/s, and transmission spectra were collected at 160 K in the dark. They were converted to absorbance difference spectra by referencing against transmission spectra measured at 160 K without prior illumination. In Figure 10a, we have plotted spectra of L29W and L29W/L104W MbCO prepared in the absence or presence of 1 atm of Xe gas. In the bands of heme-bound CO, large absorbance signals of more than 100 mOD are observed, representing a high photoproduct yield of ∼80%. Photodissociated CO in L29W displays a broad band peaking at 2130 cm^{-1}, with a pronounced shoulder at 2135 cm^{-1} and an additional bulge at 2128 cm^{-1}. The presence of Xe causes significant changes. In the region of heme-bound CO, Xe shifts the A_I-A_{II} equilibrium almost completely to A_I. The photoproduct spectrum displays two bands at 2130 and 2135 cm^{-1}, characteristic of the C″ intermediate, and the bulge at 2128 cm^{-1} is absent. In contrast, the spectrum of L29W/L104W is not affected by Xe. It shows two bands associated with A_I and A_{II} in the region of heme-bound CO and two photoproduct bands (the different spectral areas are caused by different sample concentrations). In Figure 10b, we show that the photoproduct spectra of L29W, L29W(Xe), and L29W/L104W can be decomposed into Gaussian bands at 2128, 2130, and 2135 cm^{-1}, respectively.

To monitor ligand recombination in a fluctuating protein, TDS data were collected after the described illumination protocol. TDS contour maps of L29W, L29W(Xe), and double mutant L29W/L104W MbCO are compiled in Figure 11. In L29W, recombination to A_I and A_{II} occurs at ∼190 and ∼200 K, respectively (Figure 11a). The TDS map of the photoproducts in Figure 11b reveals recombination from a broad feature at ∼2128 cm^{-1}, with a shoulder to the blue side. In the presence of xenon, recombination occurs at a temperature ∼10 K lower (Figure 11c,d), and the photoproduct map appears to be slightly more featured. For L29W/L104W, the TDS maps are similar to those of L29W(Xe). Moreover, unlike L29W, these two samples share weak features below 180 K in their photoproduct maps.

Flash Photolysis at Ambient Temperature. Figure 12 shows kinetic traces of CO and O_2 recombination to L29W Mb and related double mutants. We have also included data for wt Mb for comparison. The amplitudes of solvent rebinding (N_S) and the bimolecular rate coefficients (λ'_S) were determined by fitting exponentials to the data. These parameters are listed in Table 2 for all the mutants that have been studied. Solvent rebinding in L29W/I107W is nonexponential even at room temperature, and its kinetics were analyzed by fitting with two exponentials.

The data in Figure 12a reveal pronounced differences between wt MbCO and the mutants with an L29W replacement. In wt MbCO, a small fraction (∼4%) rebinds geminately, as seen from a slight decay below 10^{-6} s. The majority of CO ligands, however, escape to the solvent and rebind in a bimolecular reaction on the millisecond time scale (at 1 atm of CO). In contrast to wt MbCO, all our mutants with the L29W replacement show a significant absorbance increase at 436 nm below 1 μs, which is surprising because rebinding is always associated with an absorbance decrease. A small step occurs in the kinetics around $10^{-5}-10^{-4}$ s. Varying the CO concentration had no effect on the time scale of this kinetic component (data not shown), and thus, it represents geminate rebinding. A precise determination of the geminate fraction is not possible because the spectral changes at early times may be partially superimposed on the geminate step. Compared with wt MbCO, bimolecular CO binding is slowed for all L29W mutants by ∼2 orders of magnitude, with only small changes among the mutants.

Flash photolysis on wt MbO_2 shows a large, nonexponential geminate decay extending out to 1 μs. The L29W mutants show an even smaller fraction of ligands that escape to the solvent after photodissociation. Their geminate phases are faster and completely outside the time window that is accessible to our spectrometer. Bimolecular rebinding of O_2 to L29W and related double mutants is kinetically similar and significantly faster than CO rebinding. Compared with that for wt MbCO, rebinding is slower by a factor of ∼50.

DISCUSSION

Taxonomic Substates A_I and A_{II} and Their Primary Photoproducts B. The appearance of two taxonomic substates

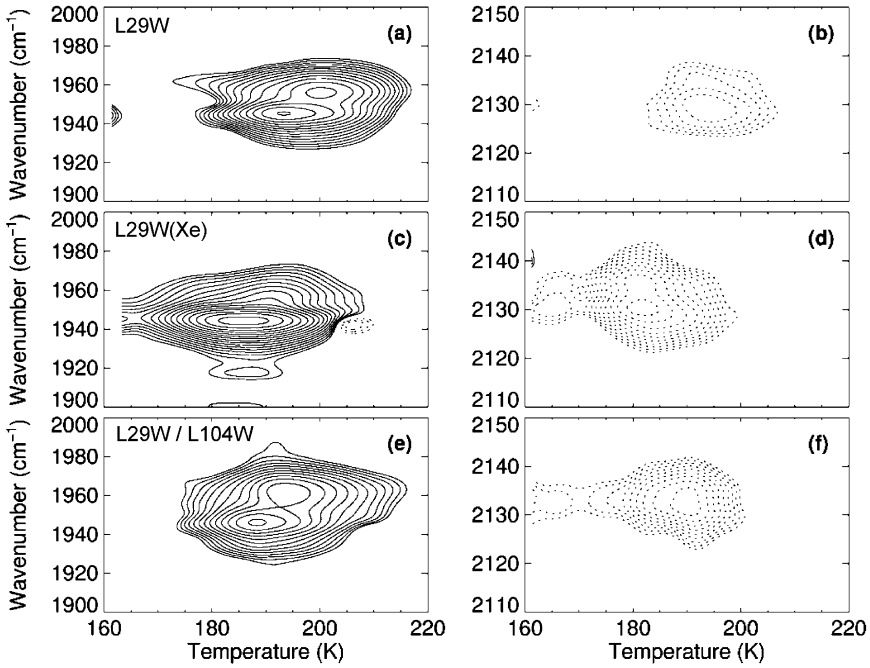

FIGURE 11: TDS contour maps of L29W MbCO in the presence and absence of Xe gas and L29W/L104W MbCO after illumination at 185 K for 2 h and subsequent slow cooling under illumination from 185 to 160 K. Absorbance changes in the IR bands of heme-bound CO are plotted in panels a, c, and e; absorbance changes in the photoproduct bands are seen in panels b, d, and f. Contours are spaced logarithmically; solid and dotted lines represent absorbance increases and decreases, respectively.

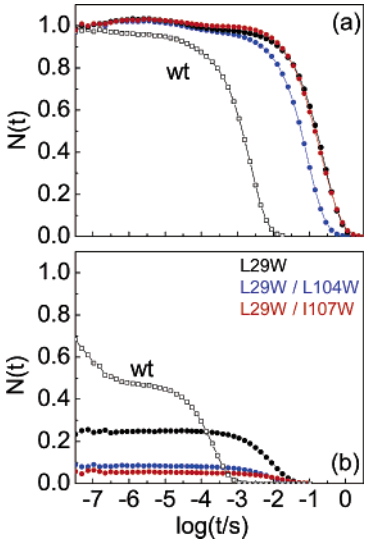

FIGURE 12: Flash photolysis kinetics of L29W and related double mutants monitored at 436 nm and 20 °C: (a) CO rebinding and (b) O_2 rebinding. Data for wt are included for comparison. Lines are shown to guide the eye.

A_I and A_{II} is typical of all mutants studied in this work (Figure 2), indicating that the W29 side chain strongly influences the stretch bands of heme-bound CO. In L29W Mb, the protein can adopt two distinctly different structures near the active site (Figure 1), which explains their markedly different primary photoproducts with respect to spectroscopic and ligand binding properties. In A_I, the W29 side chain is retracted from the heme group, leaving enough space for ligands to occupy the primary docking site B. Indeed, we have observed two stretch bands for the primary A_I photoproduct at 2122 and 2131 cm^{-1} (Figure 4), which are similar to those of wt MbCO at 2119 and 2131 cm^{-1}, respectively. Thus, we also call them B_2 and B_1, respectively (*32*, *58*, *59*). The two bands have been explained by Stark splitting of the spectrum of the CO stretch assuming opposite orientations of the CO dipole with respect to the local electric field at the docking site (*44*). In L29W, photoproduct B_2 is strongly preferred (Figure 4). As the bulky tryptophan side chain occupies a significant fraction of the distal pocket, CO rotation into orientation B_1 might be hindered. Moreover, electrostatic interactions between the aromatic indole side chain and the photolyzed ligand may favor the B_2 orientation. In the A_{II} substate, the W29 indole side chain approaches the heme group and interferes sterically with site B (Figure 1). Therefore, the CO ligands must settle in a different docking site after photolysis. Indeed, the broad IR spectrum of B(A_{II}) in Figure 4 and the featureless distribution of recombination temperatures and thus enthalpy barriers (Figure 3a) suggest that site B(A_{II}) is structurally not well defined.

Table 2: Comparison of the Bimolecular Rate Coefficients for CO and O_2 Binding to Sperm Whale Myoglobin and Selected Mutants[a]

	N_S(CO)	N_S(O_2)	λ'_S(CO) (μM^{-1} s^{-1})	λ'_S(O_2) (μM^{-1} s^{-1})
wt	0.96	0.56	0.47	16.2
L29W	~0.97	0.25	0.003	0.31
L29W/L72F	~0.97	0.13	0.001	0.18
L29W/L104W	~0.97	0.30	0.011	0.38
L29W/I107W	~0.97	0.20	0.012/0.003	0.38/0.13

[a] All data were taken at 20 °C in 0.1 M sodium phosphate buffer (pH 8).

Structural Aspects of Intermediate C′. Even at 3 K, extended illumination creates a substantial population of proteins in photoproduct state C′, characterized by two IR bands at 2127 and 2133 cm^{-1} (Figure 4), from where thermally activated recombination occurs at ~110 K on the time scale of the TDS experiment (Figure 3c,d). X-ray structure analysis of L29W crystals at 105 K (*26*, *60*) after illumination below 180 K yielded essentially all of the CO

ligands in the Xe4 cavity in a crystal that contained practically only protein molecules in the A_I conformation. Therefore, we can unambiguously assign intermediate C′ to a photoproduct with CO in the Xe4 cavity. As for the primary photoproduct, there is only one CO position in the X-ray structure, but a doublet of IR bands. We explain this result with two opposite orientations of the CO in the Xe4 cavity (*61*).

At 3 K, the enthalpy barrier for CO migration to the Xe4 cavity is too high to be overcome by thermal activation (Figure 6). Our experiments show that intermediate C′ is populated in a light-induced process at 3 K. Absorption of a visible photon at 532 nm by the heme group corresponds to a local energy deposition of 225 kJ/mol. Conversion of the phonon energy into vibrational energy raises the average temperature of the heme by several hundred kelvin (*62*). Subsequent cooling occurs within picoseconds by interaction with the surrounding moiety. Because the CO is in van der Waals contact with the heme, some of the heme energy is apparently converted into kinetic energy of the CO, enabling it to overcome the enthalpy barrier separating the Xe4 cavity from primary docking site B.

Thermal transitions, however, become significant above 100 K, as shown by time-resolved IR spectroscopy (*26*), and with a further increase in temperature, gradually more ligands escape to C′ and rebind from there. This is reflected in the Arrhenius parameters of the barriers separating state B from states A and C′. The B to A transition has both a smaller enthalpy barrier and a smaller preexponential than the B to C′ transition (*26*). At low temperatures, rebinding is governed by the lower barrier, and therefore, recombination from B dominates. At higher temperatures, however, the higher preexponential for the B to C′ transition implies that CO molecules in docking site B preferentially migrate to C′. A similar ligand migration process into the Xe4 cavity was observed at ∼35 K in myoglobin triple mutant YQR MbCO (L29Y/H64Q/T67R) which also has a bulky aromatic side chain at position 29 (*45*).

In the A_{II} substate, the W29 indole side chain is located so close to the heme group that it occludes not only site B but also the pathway to C′. Consequently, the Xe4 cavity is not accessible as an intermediate docking site for dissociated CO in A_{II} molecules, as seen from the absence of a photoproduct state C′(A_{II}) in the TDS maps.

A Protein Conformational Change Converts Photoproduct C′ to C″. Our data in Figure 8 have provided clear evidence of an additional photoproduct C″ that is spectroscopically and kinetically distinct from C′. It appears in L29W and all L29W double mutants that have been studied, which suggests that it is closely connected to the presence of W29. By introducing additional mutations, in which bulky side chains block internal protein cavities, we have determined the structural properties of this intermediate. In mutant L29W/L104W, the voluminous indole side chain of W104 occludes proximal cavity Xe1 (*63*). Yet, this mutant displays IR bands typical of C″ (Figure 9a), which rules out the possibility that the CO resides in Xe1 in this intermediate. For L29W/L72F, we would expect a strong effect on the IR spectra for CO in Xe2 because of the bulky phenylalanine side chain at this site (Figure 1). However, the C″ spectrum of mutant L29W/L72F is almost identical to that of L29W (Figure 9a), implying an unaltered environment of the ligand. Only for mutants L29W/I107W and L29W/L32T do the CO spectra assigned to C″ (and to C′) differ considerably from those of L29W (Figure 9b), which strongly suggests that residues 32 and 107 are both in close contact with the CO not only in C″ but also in C′. These residues line the back of the distal heme pocket around the Xe4 site. Therefore, we conclude that CO resides in the Xe4 cavity in both C′ and C″. But how can the spectroscopic and kinetic properties change so much if the CO stays in the same site? Apparently, the protein rearranges around the CO ligand and/or the ligand reorients within the cavity. At present, no direct structural data exist that can elucidate the difference between C′ and C″ in L29W MbCO. However, similar intermediates C′ and C″ have been observed in YQR mutant MbCO (*45*). In YQR, C′ and C″ are separated well along the temperature axis. X-ray structure analysis under photolyzing conditions above 100 K yields only C″ (unpublished results), whereas the structure at ∼40 K is entirely associated with C′ (*28*, *45*). The structural change from C′ to C″ in YQR involves movements of residues 29 and 64 deeper into the distal pocket. Whereas the movement of Y29 is minimal, Q64 shifts substantially toward the heme iron and sterically hinders recombination. In analogy to these findings, we suggest that intermediate C″ in mutant L29W is characterized by CO ligands located within the Xe4 cavity, with the protein conformation A_I partially relaxed toward the unligated (deoxy) conformation, which involves a reorientation of W29 and possibly a shift of the H64 imidazole deeper into the heme pocket.

Intermediate D in a Fluctuating Protein. Near and above 160 K, only a small fraction of proteins can be kept photolyzed in wt MbCO under continuous illumination (*16*). In contrast, illumination of the L29W MbCO mutants between 185 and 160 K leads to ∼80% photodissociated molecules (Figure 10). The photoproduct spectra of L29W, L29W(Xe), and L29W/L104W MbCO in Figure 10a appear to be rather broad, but all three can be decomposed consistently using three Gaussian bands (Figure 10b). Two of them are at 2130 and 2135 cm^{-1} and thus characteristic of photoproduct intermediate C″. We assign the third, broad band at 2128 cm^{-1} to photoproduct D, in which CO resides in the Xe1 cavity. This is supported by the photoproduct spectra in Figure 10b. In L29W(Xe), decomposition into Gaussians yields a significantly weaker band at 2128 cm^{-1} compared to that in L29W. As Xe atoms preferentially occupy site D (*29*), CO ligands have to compete with xenon atoms for the Xe1 site. Moreover, the spectral band of intermediate D is completely absent in L29W/L104W MbCO, as expected for an occluded Xe1 site. Myoglobin mutant YQR also shows a photoproduct band at 2128 cm^{-1} associated with state D (*45*). Recent investigations of photoproducts in wt MbCO in cryosolvent have shown a similar photoproduct band at 2128 cm^{-1} (*64*). This also supports this assignment because the structure (and hence the IR spectrum) on the proximal side of the heme should only minimally be altered by the L29W replacement.

In the X-ray structure of L29W MbCO crystals photolyzed above 180 K, ∼60% of the CO ligands were found in the Xe1 cavity on the proximal side of the heme (*26*, *49*). The missing fraction of ligands apparently resided in other sites with such low fractional occupancies that they remained undetected. Because CO migration to the Xe1 site did not

occur upon photolysis below 180 K, structural fluctuations must have opened transient pathways for CO to escape to site D and the solvent. Large rearrangements of H64 and W29 were observed upon ligand exit from the distal cavity (Figure 1), providing clear evidence that large-scale structural changes take place in the crystal above 180 K. In our spectroscopic data, a minor fraction of the C″ population is observed, whereas the crystal structure shows intermediate D only. This discrepancy may arise from the different illumination protocols or slight differences between crystalline and solution samples that are known to exist also for wt MbCO (*65*).

There is yet another subtle but important point that deserves discussion. Both C″ and D photoproduct intermediates exist after photodissociation above 160 K (Figure 10). Figure 11 shows that these molecules recombine at ∼190 K in the fluctuating protein. However, C″ rebinds around ∼150 K at lower temperatures when the protein is still frozen (Figure 8). These two observations can only be reconciled if the effective barrier for rebinding from C″ is substantially increased in the fluctuating protein. This may be explained in the following way. After photolysis, ligands in A_I molecules of L29W become trapped in the Xe4 cavity, forming intermediate C′, and a subsequent protein relaxation generates intermediate state C″. Below the dynamic transition temperature, only partial relaxation may occur that involves W29 in particular. In the fluctuating protein, further relaxations can occur in response to the absence of CO at the active site, involving other side chains and the backbone. Most importantly, the imidazole side chain of H64 will likely move deeper into the heme pocket and thus may occlude the active site even further so that recombination from intermediate C″ slows. This is supported by the data in Figure 11d,f. There, the typical C″ features extend from 160 K up in temperature for both samples in which CO escape to the proximal side is suppressed, namely, L29W(Xe) and L29W/L104W. It appears that the typical C″ structure forms around the CO in Xe4, and that H64 can relax to some extent even below the glass transition of the solvent, which is at ∼175 K in these samples.

It is also noteworthy to comment on the A substate features in Figure 11, which seem to show that both A substates rebind ligands at these high temperatures. As described above, W29 blocks pathways to secondary sites in A_{II}, and therefore, ligand migration into long-lived photoproduct states should not be possible in this conformation. However, if fluctuations between A_I and A_{II} are possible, the features observed in A_{II} not only may represent CO rebinding within the A_{II} conformation but also can be associated with substate exchange. As seen from kinetic studies on wt (*66*) and L29W MbCO (unpublished results), these exchange processes set in around 180−190 K on the time scale of the TDS experiment. Thus, ligands will only rebind from their secondary docking sites if the W29 gate opens as the structure fluctuates into the (deoxy) A_I conformation. Fluctuations ensure that thermal equilibrium will be maintained between the (bound-state) A_I and A_{II} conformations. Consequently, the maps in Figure 11 reflect the net effect of rebinding and equilibration in the A substates. The different temperature dependencies in the A_I and A_{II} contours result from a shift in the equilibrium between A_I and A_{II} toward A_{II} with increasing temperatures.

Ligand Binding at Physiological Temperature. Our FTIR−TDS investigation at cryogenic temperatures has provided evidence of two bound-state conformations in L29W MbCO with markedly different ligand binding properties. For A_I, multiple photoproduct intermediates exist, and the reaction surface is structured such that ligands efficiently migrate from the primary docking site to the Xe4 and Xe1 cavities. For A_{II}, the migration pathway to secondary sites is blocked. It is reasonable to assume that two conformations with similar structural properties also exist in the deoxy form of the protein. X-ray structure analysis (*26*) and the study presented here both show conformational changes after ligand escape from primary docking site B. This indicates that the deligated species assumes predominantly an A_{II}-like structure, in which W29 blocks intermediate B and the migration pathway between the active site and secondary docking sites. A comparison of oxy and deoxy Mb mutant YQR also shows an equivalent movement of Y29 with the release of O_2 (*67*). Consequently, both ligand migration and conformational changes are expected to be relevant for ligand binding in L29W Mb at physiological temperatures.

The CO rebinding kinetics of L29W in Figure 12a reveal a large fraction of solvent rebinding (close to 1), similar to that of wt MbCO, indicating that CO can escape efficiently from the protein after covalent bond rupture. Docking site B plays a key role in ligand binding and escape from the active site. The bond formation process has a low Arrhenius preexponential of $\sim 10^9$ s^{-1} because concerted motions of the heme iron, the H64 side chain, and the ligand itself are necessary for the covalent bond to form (*68*), and the primary docking site B enables the CO to reside at this location long enough for bond formation to occur. Therefore, a large geminate fraction implies a high probability that CO resides in B. For the A_I substate of L29W MbCO, we would expect a small geminate fraction because of efficient removal of CO from the primary docking site into intermediates C and D. In the A_{II} substate, the primary docking site is blocked by the W29 indole, and one may reasonably assume that geminate rebinding from alternate docking sites is less efficient. Consequently, for either of the two A substates, a large fraction of the solvent process can be expected.

The data in Figure 12a were recorded with samples in aqueous solvent, which have the majority of molecules (∼80%, unpublished data) in the A_I conformation. We know that the A_{II}-like conformation is preferred in the deoxy protein, and therefore, after the escape of the ligand from the active site, the majority of proteins change structure. We suggest that this process is seen in the increase in absorbance at 436 nm at the shortest times (Figure 12a). This feature is identical in all L29W mutants in aqueous solvent that we have investigated so far. It is, however, lacking in sol−gel samples (made from TMOS precursors), in which the proteins are arrested in the A_{II} conformation (data not shown).

All L29W mutants show a similar step on time scales of 10−100 μs after completion of the relaxation. This geminate rebinding feature arises from CO trapped in secondary sites. Because L29W/L104W also has this step, it is clear ligands do not rebind exclusively from Xe1, but (also) from Xe4. This geminate phase occurs after the relaxation, and hence, we can expect that the migration pathway to the active site is essentially blocked. We consider this blockage to be responsible for the slowing of geminate rebinding, like

solvent rebinding, by ~2 orders of magnitude compared to that of wt MbCO. Supporting evidence comes from the work of Brunori *et al*. (*28*), who observed an unusually large and very slow component of geminate NO rebinding in YQR at ambient temperature. This was interpreted as recombination from secondary sites after substantial conformational changes in residues Y29 and Q64 that were proposed to impose a substantial barrier to ligand rebinding.

Obviously, ligands can be stored in the secondary sites for a long time. This implies that ligand escape from Xe4 and Xe1 through channels not involving the distal heme pocket is highly inefficient. It appears that the pathway to the active site opens only through infrequent conformational fluctuations to an A_I-like structure so that CO can either rebind or escape from the protein through a more efficient route. Olson and co-workers have proposed that fluctuations of the protein into an A_0-type conformation, in which the imidazole side chain of H64 rotates out of the distal heme pocket, provide the most important pathway for ligand entry and exit (*69*). Since introduction of this histidine gate mechanism in 1966 (*70*), experimental data have been interpreted in its favor, for instance, the significant increase in O_2 association rates at low pH (*51*, *71*) or the large increase in the ligand association rate when H64 is mutated to smaller apolar residues (*69*, *72*−*74*). However, one has to be cautious with these interpretations because the effect of H64 is 2-fold. If the H64 imidazole swings out of the distal heme pocket, it not only opens a channel that may enable ligands to access the heme pocket but also lowers the rebinding barrier at the heme and thus enhances recombination. Consequently, other groups have argued that the histidine gate may not be the primary pathway in and out of the protein (*29*, *53*, *75*). Instead, ligands may escape through the interior of the protein by multiple transiently formed hydrophobic channels. The results presented here, however, suggest that ligand exit and entry directly through the secondary docking sites Xe4 and Xe1 are inefficient, at least for L29W mutants, and ligand migration through the distal pocket may be the most important route for ligands to enter and exit the protein.

Ligand binding from the solvent to deligated L29W Mb can also be explained by the conformational gating scenario involving the two A substates, which again highlights the crucial role of intermediate B. The deoxy species is preferentially in the A_{II}-like conformation, with its blocked primary docking site (*26*). Therefore, capturing of incoming ligands will be highly inefficient. Only a rare fluctuation to an A_I-like conformation will enable the ligand to access the primary docking site, from which the covalent bond to the heme iron can form. This picture is supported by the fact that all our L29W mutants exhibit similar behavior and rebind substantially more slowly than wt MbCO. Apparently, the conformational change involving W29 is the main determinant causing the pronounced slowing of the kinetics, and not ligand migration among internal cavities. L29W/L104W is slightly faster than the other mutants. As the geminate process is also slightly faster, this may indicate a proximal effect on the binding rates. Liong *et al*. (*63*) as well as Scott *et al*. (*69*) have shown that residue 104 is important for defining the position of the porphyrin within the protein, which in turn influences the reactivity of the heme group toward the ligands. The large tryptophan inside the proximal cavity may hinder to some extent the iron movement out of the heme plane in the photodissociated intermediate state. Since recombination reverses the protein conformational change, rebinding to a conformation that is closer to that of the ligated molecule is faster than ligand rebinding to the relaxed deoxy conformation.

The kinetics of O_2 binding are also much slower (~50-fold) for the L29W mutants than for wt Mb (Figure 12b). The similar bimolecular rate coefficients for the various mutants suggest that, as for CO, the A_I to A_{II} conformational change is responsible for the slow dioxygen binding, in analogy to the oxy to deoxy transition and concomitant slowing of recombination in the YQR mutant (*67*). Pronounced differences among the mutants are seen for the fraction of bimolecular rebinding. Oxygen (and NO) rebinding to wt Mb is complicated by the presence of a significant fraction of molecules that rebind extremely quickly (picosecond time scales) (*76*−*79*). These molecules recombine in an essentially barrierless transition so that they appear to be nonphotolyzable in experiments with nanosecond time resolution (or slower) even at very low temperatures (*2*, *78*). At present, no definitive structural explanation of these low-barrier conformations exists, although they have been associated with the linkage of the heme iron to the proximal protein moiety (*79*). The other fraction, however, behaves kinetically like MbCO (*5*).

Compared with that of CO, dioxygen rebinding to Mb generally shows an enhanced geminate process at room temperature on nanosecond time scales. This may be caused by fluctuations among the low- and high-barrier populations on even faster time scales, creating effectively a lower average barrier. The time scales of geminate rebinding are similar for CO and O_2, which suggests that ligand diffusion through and escape from the protein govern the geminate phase.

For the L29W mutants, the geminate decay at early times is absent within the time window of our spectrometer. The low photolysis yields, deduced from comparing the expected and actually observed absorbance changes at 436 nm, however, suggest significant fractions of very fast rebinders. Moreover, there are pronounced differences among the mutants. At present, one can only speculate about these variations in geminate yield among the different mutants. One could argue that a large fraction of proteins is in the fast-rebinding conformation immediately after photolysis. For electronic reasons, bond formation may be more feasible for O_2 so that a primary docking site B is less important. Then, the decreased size of the distal pocket in L29W makes it more probable that the O_2 molecule will quickly return to the active site, thus enhancing the fraction of fast rebinders. This explanation is consistent with the increased geminate yield of L29W and its double mutants as compared with those of wt MbO_2 and its respective single mutants (*64*). The increased yield in L29W/L104W compared with that of L29W may again be a result of proximal effects.

CONCLUSIONS

Using FTIR−TDS and kinetic IR experiments in combination with sophisticated illumination protocols, we have characterized a number of photoproduct intermediates for the two major substates of L29W MbCO, A_I and A_{II}, summarized in Figure 13. In the A_I conformation, state B is

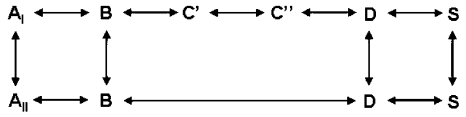

FIGURE 13: Scheme of the two ligand-bound conformations of sperm whale Mb mutant L29W, A_I and A_{II}, and their associated reaction intermediates. For details, see the text.

associated with ligands residing at the primary docking site, from which formation of a heme iron−ligand bond occurs. For the A_{II} conformation, the W29 side chain blocks access to this site, and the location of the CO is not yet known. States C′ and C″ are only observed in the A_I conformation at low temperatures; they are characterized by ligands in the Xe4 cavity. Our studies suggest that C″ differs from C′ by a local relaxation of the protein at the Xe4 site toward a more A_{II}-like structure. Intermediate D is associated with ligands in Xe1, and the deligated state is denoted with S. Below 160 K, transitions between photolysis intermediates are observed separately within the A_I and A_{II} conformations because interconversions between the two conformations are frozen in. Above 160 K, transitions between the two rows of the scheme can occur, as indicated by the arrows. We note that this scheme is *not* meant to imply that ligands must migrate sequentially through all intermediates on their way from the solvent to the active site. For instance, they may rebind via the S → B → A or S → D → B → A pathway without visiting the Xe4 site.

In the course of these investigations, a clear advantage of mutant L29W became evident. The interaction between the W29 indole side chain and the CO dipole produces large spectral changes in the bands of the CO stretch that have aided enormously in relating these changes to ligand migration and protein dynamics. As a matter of fact, the results with L29W were pivotal for understanding the rather subtle effects observed with the wt protein (*64*).

The various intermediate states were interpreted on the basis of the known photoproduct structures (*26*). The distinctly different ligand binding properties of A_I and A_{II} can be traced to different positions of the W29 and H64 side chains in the distal heme pocket. Fluctuations between the two major substates have been shown to be important in the extremely slow physiological ligand binding process. In aqueous solution, A_I is the dominant substate at room temperature. When the ligand escapes form the distal pocket, the equilibrium shifts to an A_{II}-type deligated structure, blocking access to the primary docking site from where bond formation occurs. Ligand binding occurs only through rare fluctuations to an A_I-type structure, which makes bimolecular rebinding extremely slow.

ACKNOWLEDGMENT

We thank Uwe Theilen for constructing and producing the myoglobin mutants used in this study and Dr. Don C. Lamb for discussions and technical assistance in the early stages of this investigation.

REFERENCES

1. Ansari, A., Berendzen, J., Bowne, S. F., Frauenfelder, H., Iben, I. E., Sauke, T. B., Shyamsunder, E., and Young, R. D. (1985) Protein states and proteinquakes, *Proc. Natl. Acad. Sci. U.S.A. 82*, 5000−5004.
2. Austin, R. H., Beeson, K. W., Eisenstein, L., Frauenfelder, H., and Gunsalus, I. C. (1975) Dynamics of ligand binding to myoglobin, *Biochemistry 14*, 5355−5373.
3. Brunori, M., Bonaventura, J., Bonaventura, C., Antonini, E., and Wyman, J. (1972) Carbon monoxide binding by hemoglobin and myoglobin under photodissociating conditions, *Proc. Natl. Acad. Sci. U.S.A. 69*, 868−871.
4. Frauenfelder, H., McMahon, B. H., Austin, R. H., Chu, K., and Groves, J. T. (2001) The role of structure, energy landscape, dynamics, and allostery in the enzymatic function of myoglobin, *Proc. Natl. Acad. Sci. U.S.A. 98*, 2370−2374.
5. Frauenfelder, H., and Wolynes, P. G. (1985) Rate theories and puzzles of hemeprotein kinetics, *Science 229*, 337−345.
6. Frauenfelder, H. (1978) Principles of ligand binding to heme proteins, *Methods Enzymol. 54*, 506−532.
7. Gibson, Q. H. (1989) Hemoproteins, ligands, and quanta, *J. Biol. Chem. 264*, 20155−20158.
8. Petsko, G. A. (1994) Biophysics. The little big bang, *Nature 371*, 740−741.
9. Kendrew, J. C., Dickerson, R. E., Strandberg, B. E., Hart, R. G., Davies, D. R., Phillips, D. R., Phillips, D. C., and Shore, V. C. (1960) Structure of myoglobin: a three-dimensional Fourier synthesis at 2 Å resolution, *Nature 185*, 422−427.
10. Kendrew, J. C. (1963) Myoglobin and the Structure of Proteins, *Science 139*, 1259−1266.
11. Schoenborn, B. P., Watson, H. C., and Kendrew, J. C. (1965) Binding of xenon to sperm whale myoglobin, *Nature 207*, 28−30.
12. Gibson, Q. H., and Ainsworth, S. (1957) Photosensitivity of haem compounds, *Nature 180*, 1416−1417.
13. Agmon, N., and Hopfield, J. J. (1983) CO binding to heme proteins: A model for barrier height distributions and slow conformational changes, *J. Chem. Phys. 79*, 2042−2053.
14. Agmon, N., Doster, W., and Post, F. (1994) The transition from inhomogeneous to homogeneous kinetics in CO binding to myoglobin, *Biophys. J. 66*, 1612−1622.
15. Chatfield, M. D., Walda, K. N., and Magde, D. (1990) Activation parameters for ligand escape from myoglobin proteins at room temperature, *J. Am. Chem. Soc. 112*, 4680−4687.
16. Nienhaus, G. U., Mourant, J. R., and Frauenfelder, H. (1992) Spectroscopic evidence for conformational relaxation in myoglobin, *Proc. Natl. Acad. Sci. U.S.A. 89*, 2902−2906.
17. Nienhaus, G. U., Mourant, J. R., Chu, K., and Frauenfelder, H. (1994) Ligand binding to heme proteins: the effect of light on ligand binding in myoglobin, *Biochemistry 33*, 13413−13430.
18. Steinbach, P. J., Ansari, A., Berendzen, J., Braunstein, D., Chu, K., Cowen, B. R., Ehrenstein, D., Frauenfelder, H., Johnson, J. B., Lamb, D. C., Luck, S., Mourant, J. R., Nienhaus, G. U., Ormos, P., Philipp, R., Xie, A., and Young, R. D. (1991) Ligand binding to heme proteins: connection between dynamics and function, *Biochemistry 30*, 3988−4001.
19. Chance, B., Powers, L., Zhou, Y.-H., and Naqui, A. (1986) *Bull. Am. Phys. Soc. 31*, 386.
20. Jongeward, K. A., Magde, D., Taube, D. J., Marsters, J. C., Traylor, T. G., and Sharma, V. S. (1988) Picosecond and nanosecond geminate recombination of myoglobin with carbon monoxide, oxygen, nitric oxide and isocyanides, *J. Am. Chem. Soc. 110*, 380−387.
21. Olson, J. S., and Phillips, G. N., Jr. (1996) Kinetic pathways and barriers for ligand binding to myoglobin, *J. Biol. Chem. 271*, 17593−17596.
22. Hartmann, H., Zinser, S., Komninos, P., Schneider, R. T., Nienhaus, G. U., and Parak, F. (1996) X-ray structure determination of a metastable state of carbonmonoxy myoglobin after photodissociation, *Proc. Natl. Acad. Sci. U.S.A. 93*, 7013−7016.
23. Teng, T. Y., Srajer, V., and Moffat, K. (1994) Photolysis-induced structural changes in single crystals of carbonmonoxy myoglobin at 40 K, *Nat. Struct. Biol. 1*, 701−705.
24. Schlichting, I., Berendzen, J., Phillips, G. N., Jr., and Sweet, R. M. (1994) Crystal structure of photolysed carbonmonoxy-myoglobin, *Nature 371*, 808−812.
25. Srajer, V., Teng, T., Ursby, T., Pradervand, C., Ren, Z., Adachi, S., Schildkamp, W., Bourgeois, D., Wulff, M., and Moffat, K. (1996) Photolysis of the carbon monoxide complex of myoglobin: nanosecond time-resolved crystallography, *Science 274*, 1726−1729.
26. Ostermann, A., Waschipky, R., Parak, F. G., and Nienhaus, G. U. (2000) Ligand binding and conformational motions in myoglobin, *Nature 404*, 205−208.

27. Chu, K., Vojtchovsky, J., McMahon, B. H., Sweet, R. M., Berendzen, J., and Schlichting, I. (2000) Structure of a ligand-binding intermediate in wild-type carbonmonoxy myoglobin, *Nature 403*, 921−923.
28. Brunori, M., Vallone, B., Cutruzzola, F., Travaglini-Allocatelli, C., Berendzen, J., Chu, K., Sweet, R. M., and Schlichting, I. (2000) The role of cavities in protein dynamics: crystal structure of a photolytic intermediate of a mutant myoglobin, *Proc. Natl. Acad. Sci. U.S.A. 97*, 2058−2063.
29. Tilton, R. F., Jr., Kuntz, I. D., Jr., and Petsko, G. A. (1984) Cavities in proteins: structure of a metmyoglobin-xenon complex solved to 1.9 Å, *Biochemistry 23*, 2849−2857.
30. Brunori, M., and Gibson, Q. H. (2001) Cavities and packing defects in the structural dynamics of myoglobin, *EMBO Rep. 2*, 674−679.
31. Srajer, V., Ren, Z., Teng, T. Y., Schmidt, M., Ursby, T., Bourgeois, D., Pradervand, C., Schildkamp, W., Wulff, M., and Moffat, K. (2001) Protein conformational relaxation and ligand migration in myoglobin: a nanosecond to millisecond molecular movie from time-resolved Laue X-ray diffraction, *Biochemistry 40*, 13802−13815.
32. Alben, J. O., Beece, D., Bowne, S. F., Doster, W., Eisenstein, L., Frauenfelder, H., Good, D., McDonald, J. D., Marden, M. C., Moh, P. P., Reinisch, L., Reynolds, A. H., Shyamsunder, E., and Yue, K. T. (1982) Infrared spectroscopy of photodissociated carboxy-myoglobin at low temperatures, *Proc. Natl. Acad. Sci. U.S.A. 79*, 3744−3748.
33. Frauenfelder, H., Sligar, S. G., and Wolynes, P. G. (1991) The energy landscapes and motions of proteins, *Science 254*, 1598−1603.
34. Nienhaus, G. U., and Young, R. D. (1996) *Protein dynamics*, VCH Publishers, New York.
35. Braunstein, D. P., Chu, K., Egeberg, K. D., Frauenfelder, H., Mourant, J. R., Nienhaus, G. U., Ormos, P., Sligar, S. G., Springer, B. A., and Young, R. D. (1993) Ligand binding to heme proteins: III. FTIR studies of His-E7 and Val-E11 mutants of carbonmonoxymyoglobin, *Biophys. J. 65*, 2447−2454.
36. Li, T., Quillin, M. L., Phillips, G. N., Jr., and Olson, J. S. (1994) Structural determinants of the stretching frequency of CO bound to myoglobin, *Biochemistry 33*, 1433−1446.
37. Phillips, G. N., Jr., Teodoro, M. L., Li, T., Smith, B., and Olson, J. S. (1999) Bound CO is a molecular probe of electrostatic potential in the distal pocket of myoglobin, *J. Phys. Chem. B 103*, 8817−8829.
38. Kushkuley, B., and Stavrov, S. S. (1996) Theoretical study of the distal-side steric and electrostatic effects on the vibrational characteristics of the FeCO unit of the carbonylheme proteins and their models, *Biophys. J. 70*, 1214−1229.
39. Kushkuley, B., and Stavrov, S. S. (1997) Theoretical study of the electrostatic and steric effects on the spectroscopic characteristics of the metal−ligand unit of heme proteins. 2. C−O vibrational frequencies, ^{17}O isotropic chemical shifts, and nuclear quadrupole coupling constants, *Biophys. J. 72*, 899−912.
40. Lim, M., Jackson, T. A., and Anfinrud, P. A. (1995) Binding of CO to myoglobin from a heme pocket docking site to form nearly linear Fe−C−O, *Science 269*, 962−966.
41. Mourant, J. R., Braunstein, D. P., Chu, K., Frauenfelder, H., Nienhaus, G. U., Ormos, P., and Young, R. D. (1993) Ligand binding to heme proteins: II. Transitions in the heme pocket of myoglobin, *Biophys. J. 65*, 1496−1507.
42. Jackson, T. A., Lim, M., and Anfinrud, P. A. (1994) Complex nonexponential relaxation in myoglobin after photodissociation of MbCO: measurement and analysis from 2 ps to 56 μs, *Chem. Phys. 180*, 131−140.
43. Lim, M., Jackson, T. A., and Anfinrud, P. A. (1994) Mid-infrared vibrational spectrum of CO after photodissociation from heme: Evidence for a ligand docking site in the heme pocket of hemoglobin and myoglobin, *J. Chem. Phys. 102*, 4355−4366.
44. Lim, M., Jackson, T. A., and Anfinrud, P. A. (1997) Ultrafast rotation and trapping of carbon monoxide dissociated from myoglobin, *Nat. Struct. Biol. 4*, 209−214.
45. Lamb, D. C., Nienhaus, K., Arcovito, A., Draghi, F., Miele, A. E., Brunori, M., and Nienhaus, G. U. (2002) Structural dynamics of myoglobin: ligand migration among protein cavities studied by Fourier transform infrared/temperature derivative spectroscopy, *J. Biol. Chem. 277*, 11636−11644.
46. Nienhaus, K., Lamb, D. C., Deng, P., and Nienhaus, G. U. (2002) The Effect of Ligand Dynamics on Heme Electronic Transition Band III in Myoglobin, *Biophys. J. 82*, 1059−1067.
47. Nienhaus, G. U., Waschipky, R., Nienhaus, K., and Minkow, O. (2001) in *Proceedings of the First Workshop on Biological Physics 2000* (Sa-yakanit, V., Matsson, L., and Frauenfelder, H., Eds.) pp 56−71, World Scientific, Singapore.
48. Kriegl, J. M., Bhattacharyya, A. J., Nienhaus, K., Deng, P., Minkow, O., and Nienhaus, G. U. (2002) Ligand binding and protein dynamics in neuroglobin, *Proc. Natl. Acad. Sci. U.S.A. 99*, 7992−7997.
49. Nienhaus, G. U., and Nienhaus, K. (2002) Infrared Study of Carbon Monoxide Migration among Internal Cavities of Myoglobin Mutant L29W, *J. Biol. Phys. 28*, 163−172.
50. Müller, J. D., McMahon, B. H., Chien, E. Y., Sligar, S. G., and Nienhaus, G. U. (1999) Connection between the taxonomic substates and protonation of histidines 64 and 97 in carbonmonoxy myoglobin, *Biophys. J. 77*, 1036−1051.
51. Yang, F., and Phillips, G. N., Jr. (1996) Crystal structures of CO-, deoxy- and met-myoglobins at various pH values, *J. Mol. Biol. 256*, 762−774.
52. Hirota, S., Li, T., Phillips, G. N., Jr., Olson, J. S., Mukai, M., and Kitagawa, T. (1996) Perturbation of the Fe−O_2 Bond by Nearby Residues in Heme Pocket: Observation of ν_{Fe-O_2} Raman Bands for Oxymyoglobin Mutants, *J. Am. Chem. Soc. 118*, 7845−7846.
53. Elber, R., and Karplus, M. (1990) Enhanced Sampling in Molecular Dynamics: Use of the Time-Dependent Hartree Approximation for a Simulation of Carbon Monoxide Diffusion through Myoglobin, *J. Am. Chem. Soc. 112*, 9161−9175.
54. Springer, B. A., and Sligar, S. G. (1987) High-level expression of sperm whale myoglobin in *Escherichia coli*, *Proc. Natl. Acad. Sci. U.S.A. 84*, 8961−8965.
55. Berendzen, J., and Braunstein, D. (1990) Temperature-derivative spectroscopy: a tool for protein dynamics, *Proc. Natl. Acad. Sci. U.S.A. 87*, 1−5.
56. Nienhaus, K. (2003) Spectroscopic Studies of Ligand Migration in Myoglobin, Thesis, University of Ulm, Ulm, Germany.
57. Henry, E. R., Sommer, J. H., Hofrichter, J., and Eaton, W. A. (1983) Geminate recombination of carbon monoxide to myoglobin, *J. Mol. Biol. 166*, 443−451.
58. Caughey, W. S. (1970) Carbon monoxide bonding in hemeproteins, *Ann. N.Y. Acad. Sci. 174*, 148−153.
59. Caughey, W. S., Shimada, H., Choc, M. G., and Tucker, M. P. (1981) Dynamic protein structures: infrared evidence for four discrete rapidly interconverting conformers at the carbon monoxide binding site of bovine heart myoglobin, *Proc. Natl. Acad. Sci. U.S.A. 78*, 2903−2907.
60. Ostermann, A. (2000) Untersuchung der Proteindynamik und metastabiler Proteinzustände mit Hilfe der Röntgenstrukturananlyse, Thesis, TU München, Munich, Germany.
61. Kriegl, J. M., Nienhaus, K., Deng, P., Fuchs, J., and Nienhaus, G. U. (2003) Ligand dynamics in a protein internal cavity, *Proc. Natl. Acad. Sci. U.S.A. 100*, 7069−7074.
62. Henry, E. R., Eaton, W. A., and Hochstrasser, R. M. (1986) Molecular dynamics simulations of cooling in laser-excited heme proteins, *Proc. Natl. Acad. Sci. U.S.A. 83*, 8982−8986.
63. Liong, E. C., Dou, Y., Scott, E. E., Olson, J. S., and Phillips, G. N., Jr. (2001) Waterproofing the heme pocket. Role of proximal amino acid side chains in preventing hemin loss from myoglobin, *J. Biol. Chem. 276*, 9093−9100.
64. Nienhaus, K., Deng, P., Kriegl, J. M., and Nienhaus, G. U. (2003) Structural Dynamics of Myoglobin: Effect of Internal Cavities on Ligand Migration and Binding, *Biochemistry 42*, 9647−9658.
65. Nienhaus, G. U., Chu, K., and Jesse, K. (1998) Structural heterogeneity and ligand binding in carbonmonoxy myoglobin crystals at cryogenic temperatures, *Biochemistry 37*, 6819−6823.
66. Johnson, J. B., Lamb, D. C., Frauenfelder, H., Müller, J. D., McMahon, B., Nienhaus, G. U., and Young, R. D. (1996) Ligand binding to heme proteins. VI. Interconversion of taxonomic substates in carbonmonoxymyoglobin, *Biophys. J. 71*, 1563−1573.
67. Brunori, M., Cutruzzola, F., Savino, C., Travaglini-Allocatelli, C., Vallone, B., and Gibson, Q. H. (1999) Structural dynamics of ligand diffusion in the protein matrix: A study on a new myoglobin mutant Y(B10) Q(E7) R(E10), *Biophys. J. 76*, 1259−1269.
68. McMahon, B. H., Stojkovic, B. P., Hay, P. J., Martin, R. L., and García, A. E. (2000) Microscopic model of carbon monoxide binding to myoglobin, *J. Chem. Phys. 113*, 6831−6850.
69. Scott, E. E., Gibson, Q. H., and Olson, J. S. (2001) Mapping the pathways for O_2 entry into and exit from myoglobin, *J. Biol. Chem. 276*, 5177−5188.

70. Perutz, M. F., and Mathews, F. S. (1966) An X-ray study of azide methaemoglobin, *J. Mol. Biol.*, 199−202.
71. Tian, W. D., Sage, J. T., and Champion, P. M. (1993) Investigations of ligand association and dissociation rates in the "open" and "closed" states of myoglobin, *J. Mol. Biol. 233*, 155−166.
72. Rohlfs, R. J., Mathews, A. J., Carver, T. E., Olson, J. S., Springer, B. A., Egeberg, K. D., and Sligar, S. G. (1990) The effects of amino acid substitution at position E7 (residue 64) on the kinetics of ligand binding to sperm whale myoglobin, *J. Biol. Chem. 265*, 3168−3176.
73. Springer, B. A., Egeberg, K. D., Sligar, S. G., Rohlfs, R. J., Mathews, A. J., and Olson, J. S. (1989) Discrimination between oxygen and carbon monoxide and inhibition of autooxidation by myoglobin. Site-directed mutagenesis of the distal histidine, *J. Biol. Chem. 264*, 3057−3060.
74. Carver, T. E., Rohlfs, R. J., Olson, J. S., Gibson, Q. H., Blackmore, R. S., Springer, B. A., and Sligar, S. G. (1990) Analysis of the kinetic barriers for ligand binding to sperm whale myoglobin using site-directed mutagenesis and laser photolysis techniques, *J. Biol. Chem. 265*, 20007−20020.
75. Huang, X., and Boxer, S. G. (1994) Discovery of new ligand binding pathways in myoglobin by random mutagenesis, *Nat. Struct. Biol. 1*, 226−229.
76. Petrich, J. W., Poyart, C., and Martin, J. L. (1988) Photophysics and reactivity of heme proteins: a femtosecond absorption study of hemoglobin, myoglobin, and protoheme, *Biochemistry 27*, 4049−4060.
77. Petrich, J. W., Lambry, J. C., Kuczera, K., Karplus, M., Poyart, C., and Martin, J. L. (1991) Ligand binding and protein relaxation in heme proteins: a room-temperature analysis of NO geminate recombination, *Biochemistry 30*, 3975−3987.
78. Chance, M. R., Courtney, S. H., Chavez, M. D., Ondrias, M. R., and Friedman, J. M. (1990) O_2 and CO reactions with heme proteins: quantum yields and geminate recombination on picosecond time scales, *Biochemistry 29*, 5537−5545.
79. Miller, L. M., Patel, M., and Chance, M. R. (1996) Identification of Conformational Substates in Oxymyoglobin through the pH-Dependence of the Low-Temperature Photoproduct Yield, *J. Am. Chem. Soc. 118*, 4511−4517.

BI034787S